HEFAT2014
10th International Conference on Heat Transfer, Fluid Mechanics and Thermodynamics
14 – 16 July 2014
Orlando, Florida

STEADY AND TRANSIENT CONJUGATE HEAT TRANSFER MODELING OF IGBTS SUBJECTED TO LIQUID COOLING BY A MEMBRANE HEAT SINK FOR ROLLING STOCK APPLICATIONS

Diedrichs B.* and Steinbrecher K.
*Author for correspondence
Bombardier Transportation,
Propulsion and Controls,
Technology Support,
Västerås,
Sweden,
E-mail: ben.diedrichs@se.transport.bombardier.com

ABSTRACT

A 3-D modeling technology based on Conjugate Heat Transfer (CHT) is developed to demonstrate numerically the thermal and hydrodynamic capabilities of a liquid cooled heat sink equipped with six high power semi-conductor modules of IGBT type. Calculated results are validated against experiments for three types of heat dissipating situations, where the diodes and transistors within the modules are heated simultaneously and separately. The CHT modeling is carried out with the commercially available software STAR-CCM+ from CD-Adapco. The modeling accounts for all thin materials of the thermal stack of the six IGBT modules, the thermal compound, the aluminum based heat sink with surface enlargements and turbulent coolant flow.

Encouraged by the agreement regarding numerical and experimental steady state results, a transient modeling practice is developed for the entire system. The transient modeling enables accurate and controlled studies of the thermal impedances of step responses that are often challenging to achieve in a laboratory. The novelty is the ability to return accurate time relaxation factors between heat sink and water for the whole system.

Moreover, the transient results of the step responses are used to derive equivalent circuit models of Foster type. To that end, so-called H and Y models are devised and optimized that are able to predict essential mechanisms of the thermal cross talk of diodes and transistors. Such models are important in the daily work to provide swift and accurate results of the temperature response and life length analysis of dimensioning load cycles pertinent to rolling stock applications.

INTRODUCTION

The concern for accurate predictions of junction temperatures of high power semiconductor devices used in converters for railway applications, in the daily work of Bombardier, has led to the development of efficient and detailed investigations by means of CHT calculations. This is fundamental to dependable operation over the expected lifetime of converter systems. Further, establishing time relaxation factors of integrated systems is equally important to the dimensioning of typical load cycles of, for example, Metros and Regional Rolling Stock operations.

In this paper, thermal modelling by means of Computational Fluid Dynamics (CFD) regarding the application of IGBT modules mounted on a liquid cooled heat sink referred to as Wide channel Heat Sink (WHS) is carried out and compared with a dedicated experiment. Liquid cooled heat sinks, as opposed to air cooled systems, offer efficient de-heating and minimizes the heat spread within the modules. Moreover, the possibility to carry out accurate predictions of step responses with regards to establishing the thermal relaxation factors is discussed and demonstrated. In general, fully fledged transient calculations of the cooling flow are prohibitively expensive, and therefore avoided, see for example Ref. [1]. However, the most cumbersome properties of the flow can be fixed, which mitigates the computational effort considerably to the point where such calculations become feasible for industry use. This is accomplished by reducing the problem to resolve merely the energy equation with time whilst locking the advection of the flow. Yet, CFD is indeed impractical for resolving the transient characteristics of load cycles in daily work. For that purpose equivalent circuit models are better suited. A so-called H-model of Foster type is derived and compared with a simpler derivative. The H model is capable of thermal cross talk in the base plate and heat sink. All models are optimized against the transient results of the step responses obtained with CFD.

The content of the current manuscript is as follows: Firstly, the experimental set up is described. Secondly, the prerequisites for the CFD modelling are discussed. Next, the key experimental results are outlined, followed by definitions of the thermal impedance and resistance. Thereafter, steady and transient CFD / CHT results are presented. Subsequently, the results of the equivalent circuit models are shown. Finally the results and findings are summarized in a conclusion.

NOMENCLATURE

C [Nm/kg/K] Thermal capacitance
k [W/m/K] Thermal conductivity
p [Pa] Pressure
P [W] Average power loss per IGBT module
R [m^2K/W] Interfacial thermal resistance
Rth [K/W] Thermal Resistance
t [s] Time
u [m/s] Velocity
T [K or °C] Temperature
Zth [K/W] Thermal impedance
ρ [kg/m^3] Material density
τ [s] Time relaxation
Φ [W/m^3] Viscous dissipation

Subscripts
c-h Case to Heat sink
h-w Heat sink to Water
j-c Junction to Case

Abbreviations
CFD Computational Fluid Dynamics
CHT Conjugate Heat Transfer
D2 Hottest Diode of IGBT no. 2
D6 Hottest Diode of IGBT no. 6
DI Diode Inner of IGBT no. 2
DO Diode Outer of IGBT no. 2
IGBT Insulated Gate Bipolar Transistor
TIM Thermal Interface Material
T2 Hottest Transistor of IGBT no. 2
T6 Hottest Transistor of IGBT no. 6
TI Transistor Inner of IGBT no. 2
TO Transistor Outer of IGBT no. 2
WHS Wide channel Heat Sink

EXPERIMENTAL SET UP

The experimental consist is shown in Figure 1a. The set up uses six IGBTs mounted on a liquid cooled aluminum heat sink (WHS). Two kinds of IGBT models from the manufacturers Infineon and Hitachi are used. This study focuses attention on the results obtained with the IGBTs from Infineon labelled FZ1500R33HE3, rated for 3300 V and 1500 A, which are mounted on the lower part of the heat sink in Figure 1a of the experiment, close to the water inlet. In particular, much of this paper discusses the results obtained with IGBT no. 2. The modules are connected in series with bus bars of copper of 170 mm^2, depicted in Figure 1b. The electric current and voltage drop over the six IGBT modules in series are measured for the purpose of establishing the power losses. The electric feeding device produces AC or DC± currents, which controls the dissipated heat of the diodes and transistors. The transistors are fully modulated with 18 V over the gate. At 50 Hz AC power supply, both the diodes and transistors are subjected to an R.M.S current of about 950 A. This gives a current density of 5.6 A/mm^2 in the bus bars. The corresponding total dissipated power, P, is 1950 W for the Infineon IGBT no. 2. At DC supply only the diodes or the transistors are dissipating heat depending on the electric polarity. The average power losses for the diodes and transistors of IGBT no.2 with respect to the power supply practised herein are listed in Table 1. The power losses of Case 2 and 3 are chosen such that the case temperatures of the active chips of the diodes and transistor are somewhat similar to that of Case 1, shown in Figures 9a-c.

Case	Power supply	Diodes: *P*	Transistors: *P*
1	AC 50 Hz	955	995
2	DC+	1378	0
3	DC-	0	1624

Table 1 Total power loss P in [W] of Diodes and Transistors for IGBT no.2 with respect to the power load situation.

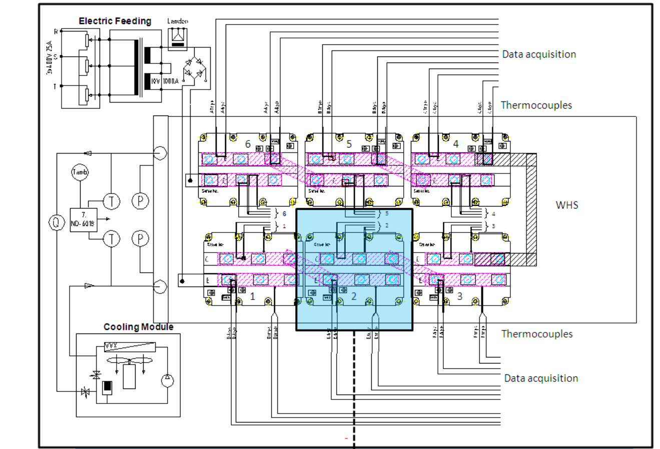

a)

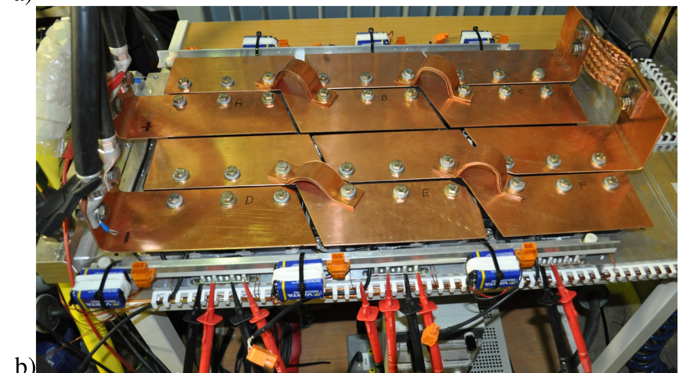

b)

Figure 1 a) Experimental set up consisting of WHS, six IGBT modules, cooling module, electric feeding device, 48 thermocouples and data acquisition unit. b) IGBT modules are connected in series with copper bus bars.

The placements of the four thermocouples inside the base plate of the Infineon module are shown in Figures 2 and 3. The thermocouples are placed inside Ø1 mm cavities 0.75 mm from the face of the base plate, see also Figures 5 and 8.

The WHS is designed for a coolant flux of 0.04 m^3/minute. This gives a flow speed inside the liquid duct of about 2 m/s, discussed in connection to Figure 7b. Six turbulence enhancers are mounted inside the duct to improve the rate of heat transfer. Inlet temperature of the coolant is fixed to 65 °C, where the flow direction changes after passing the U-turn, shown in Figure 4. With the current flow rate and power losses of Case 1, see Table 1, the coolant temperature is therefore predicted to increases 0.805 K and 4.83 K per module and totally for all six modules, respectively.

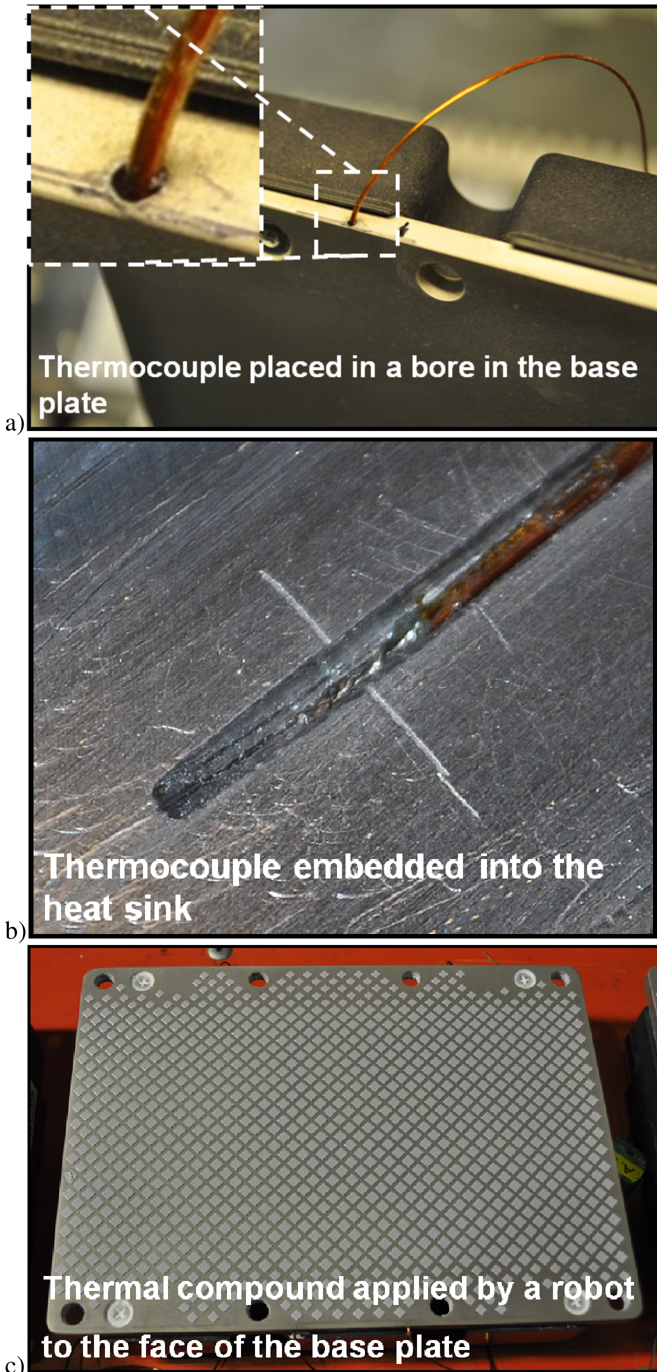

a) b) c)

Figure 2 a) Thermocouple bore axes in the base plate of the IGBT modules. b) Thermocouples embedded in the WHS. c) TIM applied to the base plate.

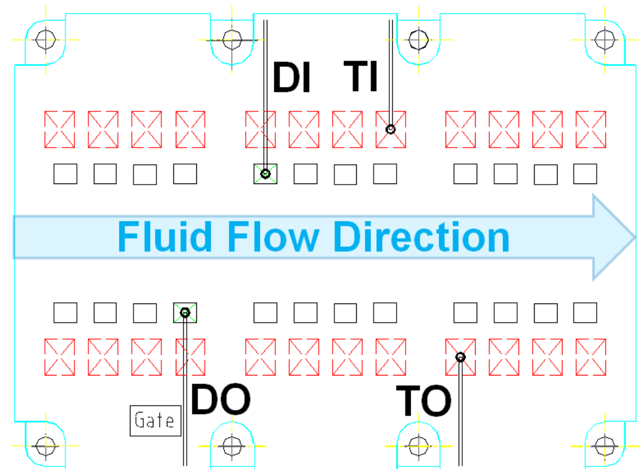

Figure 3 Placement of thermocouples in the base plate of FZ1500R33HE3 module from Infineon.

THERMAL IMPEDANCE AND RESISTANCE

The following definitions regarding thermal impedance are used:

$$Zth_{j-c} = \frac{T_j(t) - T_c(t)}{P} \quad (1)$$

$$Zth_{c-h} = \frac{T_c(t) - T_h(t)}{P} \quad (2)$$

$$Zth_{h-w} = \frac{T_h(t) - T_w(t)}{P} \quad (3)$$

T_j, T_c, T_h, T_w and t describe the temperature of junction, case (base plate), heat sink, water and time, respectively. The corresponding thermal resistances, *Rth*, are obtained in the limit of $t \to \infty$.

CFD MODELLING AND PREREQUISTES

A complete CAD database of the thermal stack of six IGBTs, WHS and coolant flow is assembled, as depicted in Figure 4, which is the basis for generating the computational mesh. The commercial software STAR-CCM+ v8.04 from CD-Adapco, based on Finite Volume Method, is utilized in the current study, which is suitable for multi physics and multi region analysis that exploits parallel computing.

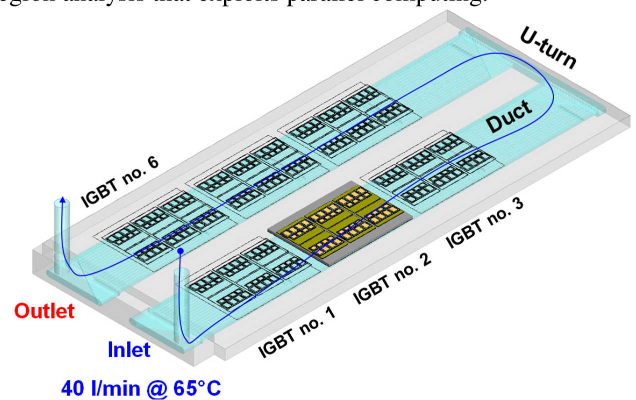

Figure 4 CAD database consisting of thermal stack of IGBT modules, WHS and coolant.

The thin thermal stack of the IGBTs is shown in Figure 5. It consists of seven layers, detailed in Table 2, each with different thermal properties. The pertinent CAD data are obtained by Courtesy of Infineon.

Interfacial thermal resistance between the base plate and WHS is applied to resolve the characteristics of the TIM. In this work the passive edge (termination) about the transistors and diodes are taken into account. The model is prepared as such that different power losses can be given to all of the transistor and diode chips. Therefore, the model contains a total of 6×2×24 = 288 volumetric heat source elements that can be controlled individually. However, in this work the power losses are equal and according to Table 1.

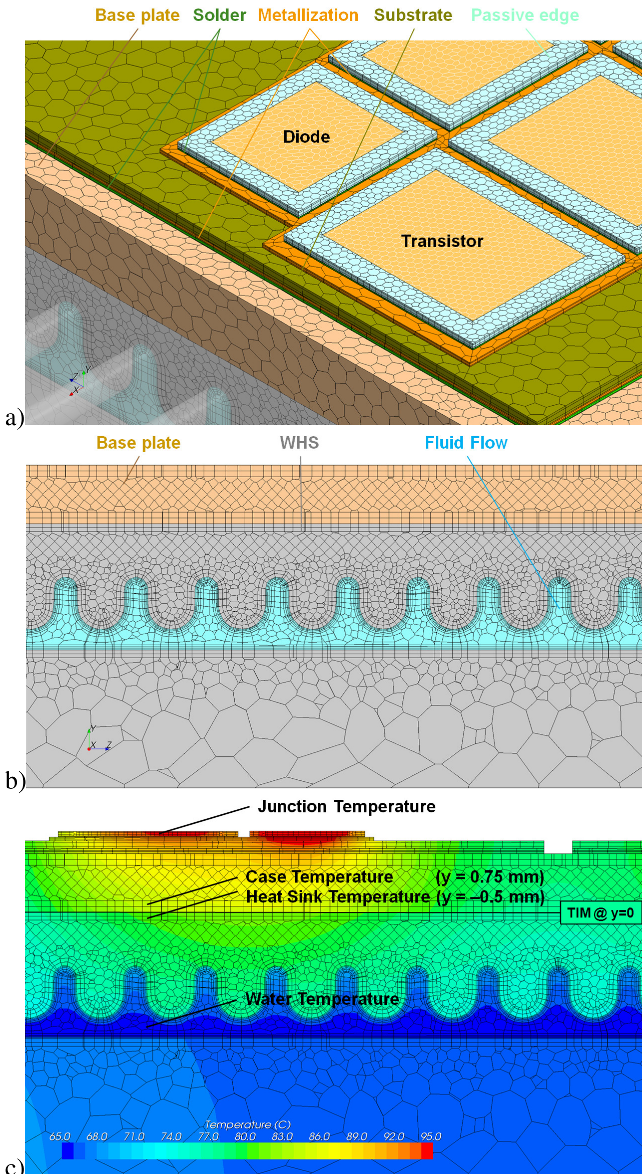

Figure 5 a) Polyhedral mesh of the thermal stack that consists of seven layers, see Table 2. b) Section of the mesh of the WHS and liquid flow underneath the IGBT module. c) Location of temperature probes for Junction, Case, Heat Sink and Water.

Physics Region	Material
Coolant	Glycol 52/48
WHS	Aluminum
TIM	TC 5021 Dow Corning®
Base plate	AlSiC
Solder	SnAgCu
Metallization	Cu
Substrate	Si3N4
Metallization	Cu
Solder	Pb(SnAg)
Transistor / Diode	Si

Table 2 Physics Regions and adherent Materials.

With the current flow properties, a so called low-Reynolds mesh, see Ref. [2] is generated inside the coolant duct with four prismatic cell layers with a total thickness of 0.49 mm, shown in Figures 5a-b. Prisms are grown into the fluid adjacent to the solid walls. Accurate CHT calculations require a low-Reynolds mesh that is conformal with respect to fluid-solid interfaces. In the current software this is achieved by using polyhedral cells. Such cells have typically twice the number of faces compared to conventional hexahedral cells. This is advantageous for complex geometries and they further augment the convergence characteristics.

The model consists of a total of 1015 physics regions, where the computational mesh consists of 29 Million polyhedral cells. 14 million cells are used to model the coolant flow in the liquid duct.

The turbulent flow is described by the Navier-Stokes equations, see Ref. [2], in conjunction with a two equation k-ω model of Menter, see Ref. [3], with a shear stress transport term. The model is referred to as k-ω SST Menter in the sequel. In addition, a realizable k-ε model, see Ref. [4], using a so-called two layer all y+ wall treatment is also used. The realizable k-ε model is claimed to be substantially better than the standard k-ε model. The latter was also attempted without success, causing the results to fluctuate with time. It will be shown that the data obtained with k-ω SST Menter resulted in the best overall agreement with the experimental data.

The flow is solved with a second order accurate scheme regarding the advection terms of the momentum and turbulence equations.

Finally, the temperature field is essentially described with the thermal energy equation:

$$\rho C \frac{DT}{Dt} = -\nabla \cdot \vec{q} - p(\nabla \cdot \vec{u}) + \Phi \qquad (4)$$

ρ, C, p, $\vec{u}$ and Φ denote density, heat capacity, pressure, velocity field and viscous dissipation. The flow is incompressible why the second term on the right hand side of Equation 4 is zero. Finally, the material derivative on the left hand side of Equation 4 includes the advection term. The heat flux obeys the Fourier law:

$$\vec{q} = -k\nabla T \qquad (5)$$

where k is the thermal conductivity. Recall that ρ, C, Φ and k are dependent on the temperature, which is accounted for in the current calculations.

Two prism layers with a total thickness 0.67 mm and 1 mm are generated inside the solids of the WHS adjacent to the duct and base plates, respectively, see Figure 5c. The temperature probes of the CFD model regarding case and heat sink data will therefore precisely read the cell centered values without the need for interpolation of data from adjacent cells. Thus, the probes of the base plate are at 0.75 mm from the face, whilst those of the heat sink lie 0.5 mm underneath the face of the WHS.

The thin layers of the thermal stack are generated with a so-called thin meshing technology that uses polyhedral cells as well. All solid materials of the thermal stack are generated with at least three cell layers, see Figure 5, which is required to properly resolve the energy equation. A prior internal study, not shown here, with only solid materials, resulted in good agreement regarding the heat transfer and corresponding time dependent temperature fields with similar settings. This work is an extension of that study and hinges on the resolution of the heat transfer of the heat sink to the coolant flow.

All walls of the solids are treated as adiabatic, which implies that all power losses of the IGBT modules are expelled through the coolant flow. This is a fair approximation, where the experiment reveals that 95% of the losses are expelled by the coolant. Typically, the maximum temperature inside the cooling compartment of the real application is often closer to the maximum coolant temperature of 65 °C rather than room temperature. Thus heat leakages in the real situation are relatively smaller. A 5% discrepancy of the power losses is estimated to impact the junction, case and heat sink temperatures with 1.5 K, 0.9 K and 0.7 K, respectively. Further, the terminals on top of the IGBT modules may act as a heat sink or heat source dependent on the current density. By measuring the power losses expelled by the coolant relative to those generated by the chips of the IGBTs, it is found that the system is at balance at about 750 A. Thus, at the current densities used herein, i.e. R.M.S. 950 A, the terminals will add power to the system and thus compensate for some of the heat that is leaked to ambient.

KEY EXPERIMENTAL RESULTS

Many of the objectives and details of the experimental investigation go beyond the scope of the current manuscript. However, to give an insight into the experimental investigation carried out under the aegis of the current development project it is mentioned that the following issues are investigated: i) Study the thermal performance of all IGBTs, ii) how thermal properties vary with power losses, iii) implications of the system pressure for the current WHS in conjunction with the thermal expansion and performance of the TIM, iv) relationship between total heat losses, losses of the chips and terminals and losses expelled by the coolant flow.

Key experimental results for this study are the measured temperatures, thermal resistances and associated scatter for the assembly of WHS and IGBT no. 1-3, i.e. of the Infineon modules. The scatter reveals deviations that may occur in real field situations and gives an understanding of the accuracy of the obtained experimental data to which the following calculations are compared. In this regard, Figures 6a-b displays the thermal resistances for IGBT no.1-3.

The relative scatter in $Rth_{c\text{-}h}$ compared to $Rth_{h\text{-}w}$ is higher due to smaller temperature differences, c.f. Equation (1). To appreciate the temperature differences the results of each group composed of Transistor Outer, Transistor Inner, Diode Outer and Diode Inner (TO, TI, DO, DI) for the three IGBTs are averaged. The absolute temperature differences from the averages denoted $\overline{T}$, i.e. $abs(T-\overline{T})$, are presented in Figures 6 c-d. In addition, the mean of the above deviations are highlighted with dashed lines. Apparently, the case temperature of TI for IGBT no. 3 resulted in a quite low thermal resistance, for unknown reasons. If that value is taken out of account the mean of the deviations regarding the case to heat sink temperatures is closer to 0.45 K. It should also be noticed that the thermal resistance of DO regarding IGBT no. 2 is greater than its neighboring data and therefore may be erroneous to some extent. The sensitivity of the placements of the thermocouples is further discussed in connection to the steady state CFD results.

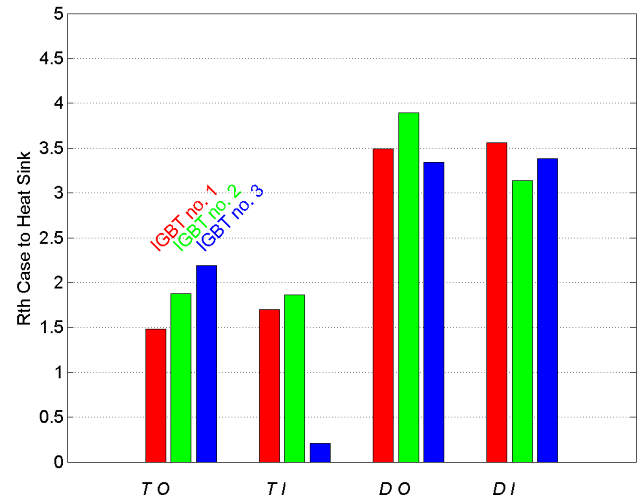

a)

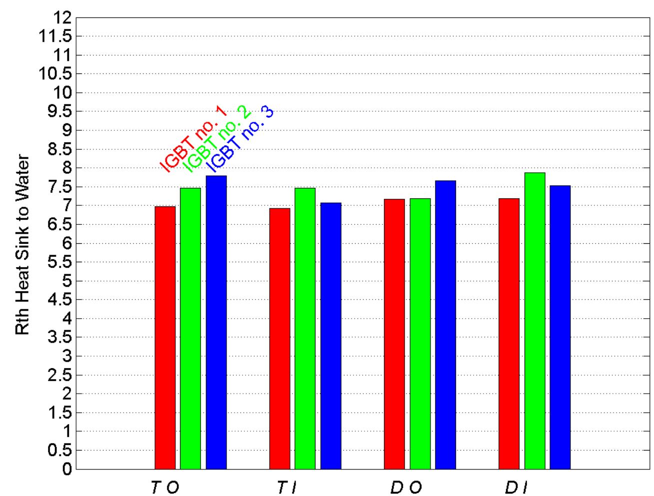

b)

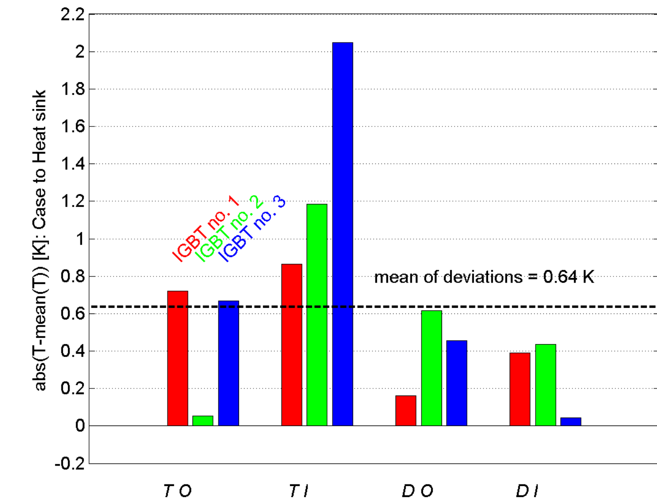

c)

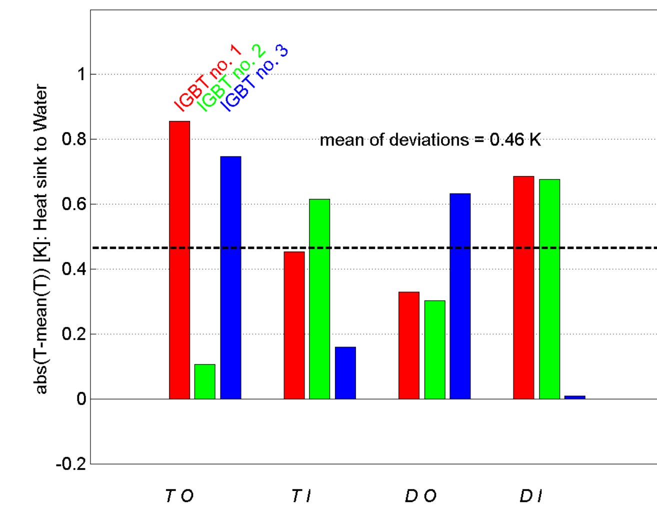

d)

Figure 6 Scatter in thermal resistances and corresponding temperatures regarding the transistor and diode chips of IGBT no. 1-3. a) $Rth_{c\text{-}h}$, b) $Rth_{h\text{-}w}$, c) $abs(T-\overline{T})_{c\text{-}h}$, d) $abs(T-\overline{T})_{h\text{-}w}$.

RESULTS OF STEADY CALCULATIONS WITH CFD

In this section, steady state calculations for the three cases of Table 1 are carried out. A fully converged calculation is obtained in approximately 15 hours of wall time on 40 computational cores on a modern main frame. All steady calculations are listed in Table 3. The sensitivity with respect to the TIM thickness and turbulence model used for the coolant flow is investigated by Calc no.1-4. In this regard, TIM thickness of 82 μm gives an Interfacial Thermal Resistance of $R = 2.4848 \times 10^{-5}$ m^2K/W. The latter TIM thickness is appreciated from the density, mass and surface area of the applied grease, illustrated in Figure 2.

Calc no.	Case	TIM thickness [μm]	Turbulence model
1	1	0	k-ω SST Menter
2	1	50	k-ω SST Menter
3	1	82	k-ω SST Menter
4	1	50	k-ε Realizable
5	2	82	k-ω SST Menter
6	3	82	k-ω SST Menter

Table 3 Steady calculations.

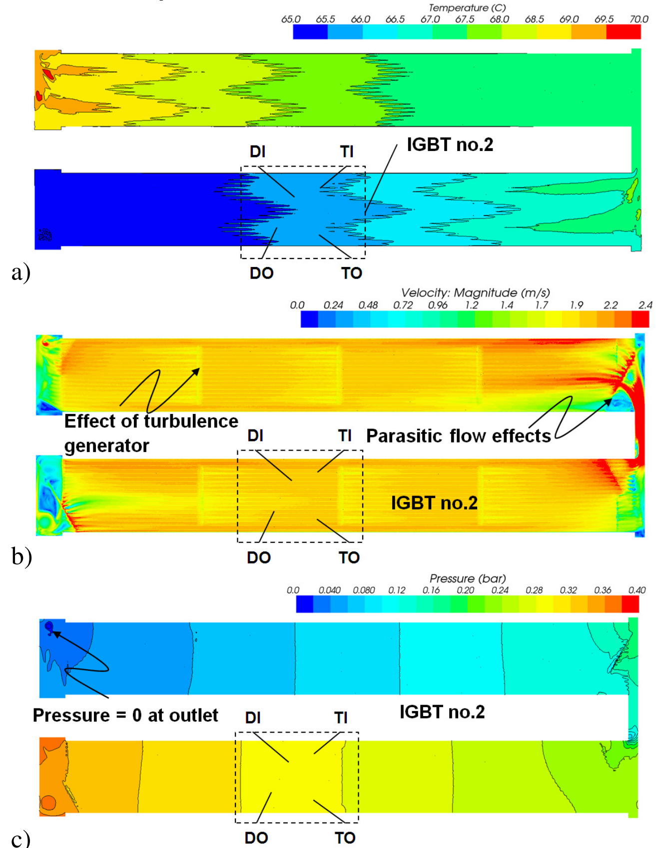

Figure 7 Flow properties of Calc no.3. a) Temperature field, b) velocity magnitude and c) pressure.

The results detail the flow properties in the duct such as the velocity field, pressure and temperature distributions, shown in Figure 7. In addition, the conjugate temperature field and corresponding heat flux is resolved in all solid materials.

The results of the calculations agree well with those of the experiment, illustrated in Figures 7a-c. For example, for Case 1, see Table 1, the temperature rise of the coolant per IGBT is 0.81 K, which gives a total of 4.9 K as it passes through the WHS, see Figure 7a. The heat transfer to the coolant from the IGBT gives a clear imprint in the temperature field in the stream-wise and cross-flow directions. It can also be discerned that the uniform temperature profile is restored due to the mixing of the fluid as it passes through the U-turn of the WHS. The velocity magnitude is illustrated in Figure 7b, where the effects of the turbulence enhancers and U-turn are most

palpable. At this point, the strengths of the CFD tool are immediately manifested by providing detailed results and ideas of how to improve the design in future applications. It goes without saying that similar illustrations of the flow results are challenging to achieve in the laboratory at a comparable cost. Moreover, the pressure drop caused by the heat sink at the current flow rate is calculated to approximately 0.4 bar, which agrees well with the experimental finding.

Temperature fields for the three cases of Table 1, i.e. Calc no. 3,5,6, are shown in Figures 8a-d. Figure 8a illustrates the external temperature of the WHS and thermal stack of the IGBTs with view from above. The cold inlet, warm outlet and increasing temperature in the stream-wise direction about the duct can be discerned. Figures 8b-d show the temperature in the cross section normal to the direction of the flow through DI. The color range is confined between 82 and 92 °C. From a three-dimensional point of view, the almost point like heat sources produce gradients of the temperature that resembles half spheres. This explains why it is notoriously difficult to measure correct temperatures inside the base plates for liquid cooling. A slight mismatch of the probe's location in either lateral or vertical direction may offset the temperature. It can further be observed that the vertical temperature gradient in the 5 mm thick base plate is approximately 1.4-1.7 K/mm for the three cases, see Figures 8b-d.

The results of the sensitivity study of Case 1 in terms of Junction, Case and Heat Sink Temperatures of TO, TI, DO and DI are shown in Figure 9a. The greatest discrepancy in junction temperature is 2.8 K for DI comparing results of zero and 82 μm thickness of TIM.

The corresponding difference for Calc no.2 and Calc no.4, i.e. effect of turbulence model, is 1.8 K. As discussed earlier, it is conjectured that the calculations may give slightly higher temperatures compared to the experimental data as a result of using adiabatic walls and neglecting thermal radiation. However, the results obtained for Case no. 3, which is our reference calculation, show differences in heat sink temperatures of –0.1 to 1.1 K compared to the experimental data.

The case temperature of DO exhibits the largest discrepancy, perhaps caused by a slightly misplaced thermocouple. In fact, it is more likely that the recorded temperature should be similar to that of DI, as this would agree with the trend of the corresponding heat sink temperatures and CFD results. This shortcoming was revealed after the test campaign had finished and is therefore not corrected. The DO case temperature of IGBT no. 2 should therefore be taken out of account.

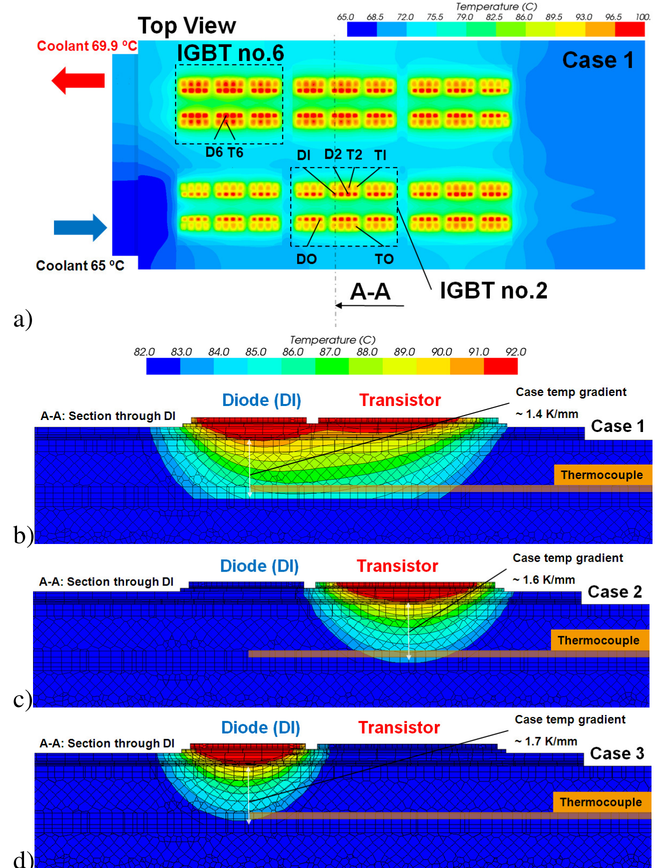

Figure 8 Temperature fields of Calc no.3,5,6. a) WHS and IGBTs from above. b,c,d) Cross section A-A through DI. Note that the temperature color bar is confined between 82 and 92 °C.

Figures 9b-c display the results of the Cases 2-3, where the calculations show fair agreement with the experimental findings. Again the case temperature of DO exhibits the largest discrepancy. The power losses of Case 3 in the experiment are adjusted such that the case temperatures of the active chips are similar to that of Case 1. For the diodes of Case 2 the similar procedure is used but the data reveals that more power losses are needed to give a perfect match. Nevertheless, the thermal cross heating yields higher temperature differences between the passive and active chips for Case 2. For example, the case temperature differences between TI and DI are 8.6 K and 6 K for Case 2 and Case 3, respectively.

Early predictions of the junction temperatures by utilizing data specifications from the supplier and measured case temperatures suggested higher values than predicted by CFD. This misconception is due to the fact that the case temperatures of the supplier really refer to the face of the base plate. In addition, a margin of 20% may be added to the thermal resistances by the manufacturer of these modules.

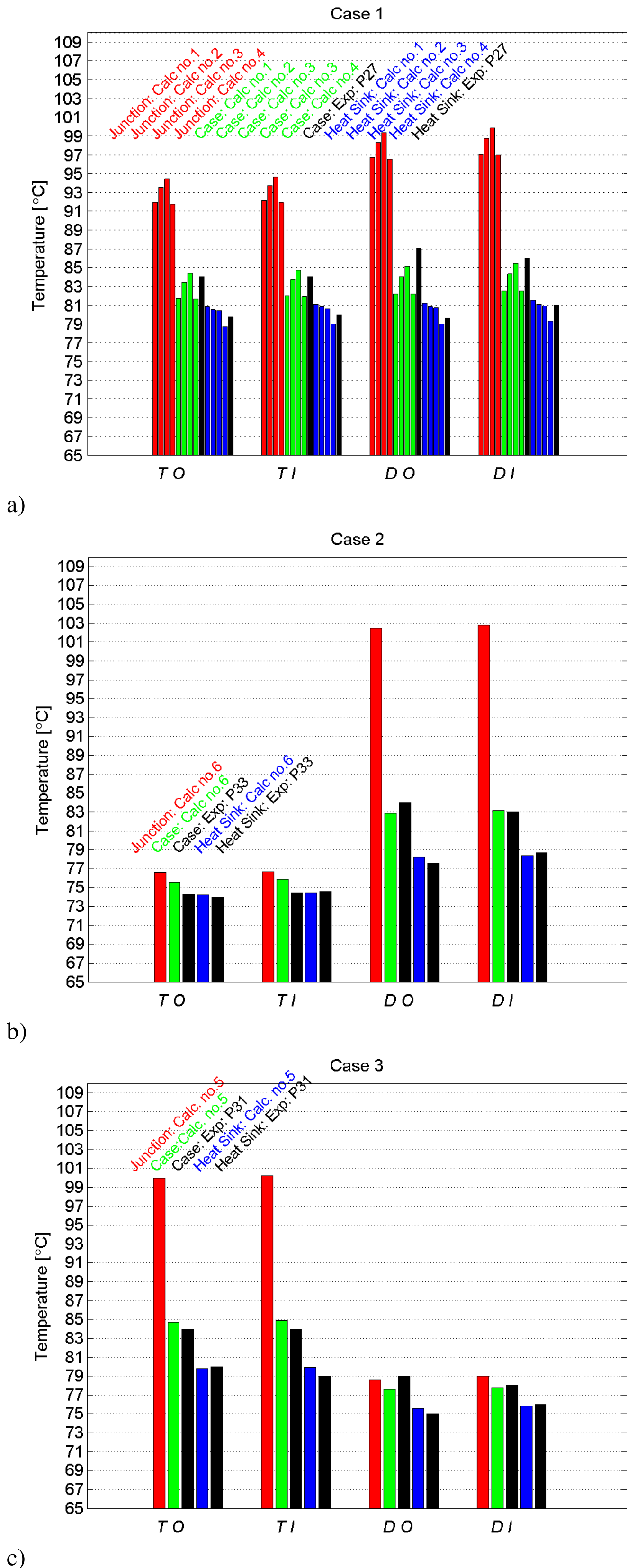

Figure 9 Temperatures at junction, case and heat sink obtained with CFD compared with experimental data.

RESULTS OF TRANSIENT CALCULATIONS WITH CFD

The objective of the current section is to demonstrate how to derive the time relaxations (τ) of the WHS and IGBTs with regards to thermal impedance data obtained from upward and downward step responses, referred to as power up and power down, respectively. As heat conduction and specific heat of the materials of Table 2 are temperature dependent, the power up / down situations should give slightly different results due to differences in the initial and developing temperatures.

The crux of the matter as far as the transient calculations are concerned is the time resolution of the turbulent liquid flow. As cell sizes of the fluid are typically in the order of one millimeter and the flow speed is mostly 2 m/s, see Figure 7b, the calculation would require the time step to be confined below 0.5 ms in order to respect the Courant condition, see for example Ref. [3]. Apparently, the required time step for the fluid calculations are at least 10 times smaller compared to what is needed initially to resolve the effects on the temperature field due to power up / down. At later times, that difference becomes much larger. It is desired to calculate data for about 100 s, in order to succeed with optimization of the RC Networks, described in the next section. Therefore, it is likely that more than 2 million time steps must be undertaken to finish the task. Moreover, approximately 5 iterations per time step are needed to achieve sufficient convergence. That would give a staggering total of 10 million iterations on a mesh with 29 million cells. Today, this is prohibitively expensive for the current industry application. Yet, the chaotic character of the turbulent flow may require the results to be ensemble averaged through a collection of runs. If so, this would for sure deteriorate the prospects of accurate transient's calculations for the current application for many years to come.

An alternative approach devised and practiced here readily locks the converged steady flow solution with respect to the momentum and turbulence equations. This admits the use of a time step that is relevant for the resolution of the temperature field as opposed to the flow field, where only the energy equation, see Equation (4) that resolves the temperature needs to be updated. In addition, the issue of using ensemble averaged data is also mitigated as the unsteady solution of the temperature field will at all times be based on the steady and thus ensemble averaged flow. This convenient trick results in an accurate and affordable approach.

It should be pointed out that the energy equation takes into account the advection of the flow field. This means that the fluid that is heated up adjacent to an IGBT will be transported in the stream-wise direction and affect the next IGBT and so forth. This is then different from transient studies that do not account for the flow effects in the system. As the inlet temperature is fixed the current calculations provide eminent conditions for evaluations of the time relaxation factors in contrast to laboratory tests, where the inlet temperature may start to drift soon after the onset.

Results from two steady calculations are used as the basis for the transient calculations, namely Calc. no.3 of Table 3 with and without applying the power losses. The time marching procedure to resolve Equation (4) utilizes a second order implicit scheme. At the onset, which occurs at t_c = 0.1 s, the

time step Δt_c is confined to 5 ms. The index c refers to the calculation time, where $t = t_c - 0.1$, used in Figure 10. Thus, 18 time steps are carried out before the transition in power losses occurs. For $1 < t_c < 10$ sec Δt_c = 10 ms and finally for $t_c \geq 10$ sec Δt_c = 20 ms. To check the sensitivity of the time step, one calculation is carried out with the minimum time step Δt_c = 2 ms. Thus, in total, five transient calculations of step responses are carried out that are listed in Table 4.

Calc no.	Case	Power	min(Δt_c) [ms]
7	1	Up	2
8	1	Up	5
9	1	Down	5
10	2	Up	5
11	3	Up	5

Table 4 Transient calculations of step responses.

Figure 10 plots the effects of the power up in terms of the temperatures and thermal impedances of Equations (1-3) for the transistor and adjacent diodes of IGBT no. 2, tagged and handled as D2 and T2, see Figure 8a. Notice that the lateral placements of these chips are different from that of the experiment and steady calculations, selected in order to capture effects of the thermal cross talk. The CFD results are used in the next section as a basis for the Foster models of H^2, Y^2 and Y^1. The experiment did not attempt such a set up due to practical reasons.

The time relaxation factors (τ) measures the time for a 63% change, really e^{-1}–1, of the thermal impedance data of Figure 10.

Results in terms of the time relaxations are listed in the Tables 5-7 for the Cases 1-3, respectively. The corresponding data from the supplier is found in Ref. [5]. Data for the thermocouples of IGBT no. 6, see Figures 4 and 8a, are included as well. The following observations are commented:

Firstly, Table 5 concludes that the results of varying the time step between 2 and 5 ms show hardly any differences. This motivates the use of the larger time step of 5 ms for all subsequent calculations.

Secondly, the results regarding the levels of junction to case, i.e. $\tau_{j\text{-}c}$, agree well with the supplier data, see Tables 6-7. At these levels, the results of the diode and transistor of IGBTs no.2 and no.6 agree very well. Actually, the differences are within the accuracy of the time step Δt_c = 5 ms.

Thirdly, at the next level of case to heat sink, i.e. $\tau_{c\text{-}h}$, the calculations are consistent in that the power down gives trifling shorter times for all chip positions. In contrary, the corresponding results for heat sink to water, i.e. $\tau_{h\text{-}w}$, are consistent in that the power down gives slightly longer times. Recall that this is an effect of the temperature dependency on the specific heat and thermal condition. Typically, a material with increasing specific heat and decreasing thermal conductivity with temperature would exhibit longer time relaxations in the power down situation.

Fourthly, $\tau_{h\text{-}w}$ for D6 and T6 are consistently greater. The reason for that is the increasing water temperature caused by the upstream IGBTs, which obviously compresses the temperature difference and thus the *Zth* initially. This effectively gives slightly longer relaxation times.

Finally, the effect of thermal cross talk in terms of time relaxation is shown as well, in Tables 6-7. Data reveals that the time relaxations are in the range of 1.56 to 2.51 s for the passive chips.

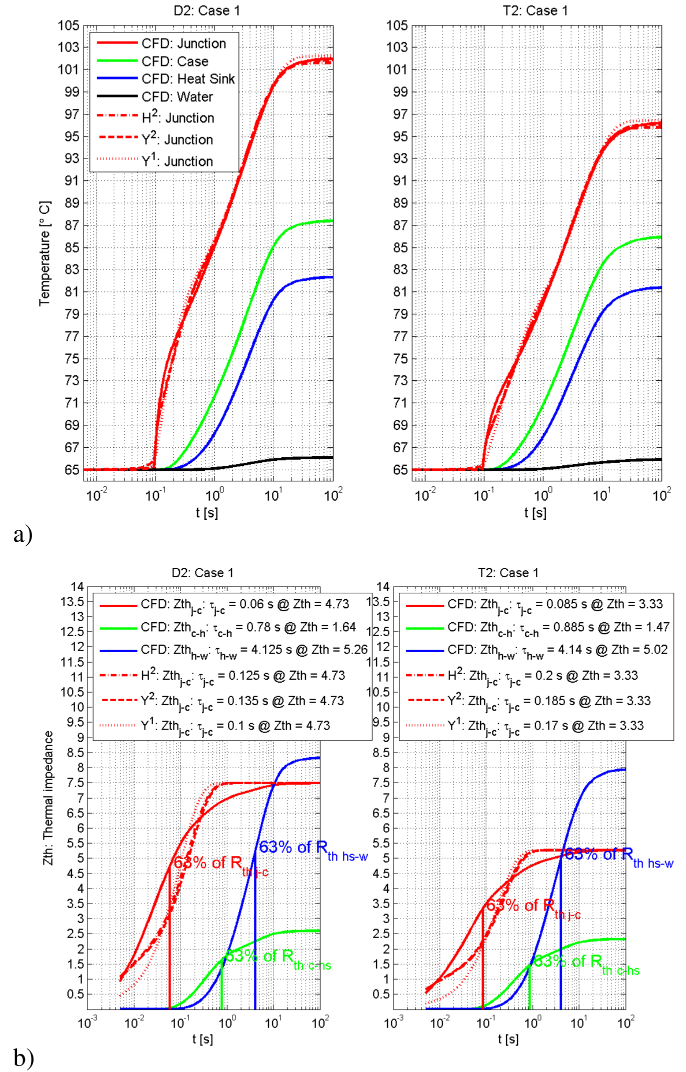

Figure 10 Power up for IGBT no. 2. a) Temperatures. b) Thermal impedances and corresponding time relaxations for the adjacent diode and transistor.

	D2-active			D6-active		
Power	Up	Up	Down	Up	Up	Down
Δt_c [ms]	2	5	5	2	5	5
$\tau_{j\text{-}c}$	0.065	0.06	0.055	0.065	0.065	0.06
$\tau_{c\text{-}h}$	0.785	0.78	0.775	0.775	0.77	0.765
$\tau_{h\text{-}w}$	4.125	4.125	4.135	4.67	4.685	4.705
	T2-active			T6-active		
Power	Up	Up	Down	Up	Up	Down
Δt_c [ms]	2	5	5	2	5	5
$\tau_{j\text{-}c}$	0.09	0.085	0.085	0.085	0.085	0.08
$\tau_{c\text{-}h}$	0.89	0.885	0.88	0.85	0.85	0.845
$\tau_{h\text{-}w}$	4.14	4.14	4.155	4.615	4.625	4.645

Table 5 Time relaxations in units of [s]. Calc no.7, 8 and 9.

	D2-active	D6-active	D Supplier
Power	Up	Up	Up
$\tau_{j\text{-}c}$	0.05	0.055	0.058
$\tau_{c\text{-}h}$	0.555	0.54	-
$\tau_{h\text{-}w}$	3.615	3.98	-
	T2-passive	T6-passive	
$\tau_{j\text{-}c}$	1.945	2.415	
$\tau_{c\text{-}h}$	2.445	2.465	-
$\tau_{h\text{-}w}$	4.88	5.62	-

Table 6 Time relaxations in units of [s]. Calc no.10.

	D2-passive	D6-passive	T Supplier
Power	Up	Up	Up
$\tau_{j\text{-}c}$	2.09	1.56	-
$\tau_{c\text{-}h}$	2.175	2.51	-
$\tau_{h\text{-}w}$	4.86	5.745	-
	T2-active	T6-active	T Supplier
$\tau_{j\text{-}c}$	0.065	0.07	0.073
$\tau_{c\text{-}h}$	0.605	0.585	-
$\tau_{h\text{-}w}$	3.58	3.875	-

Table 7 Time relaxations in units of [s]. Calc. no. 11.

RC NETWORKS OF FOSTER TYPE

In the diurnal work of designing converters for rail applications, fast and accurate predictions of the junction temperatures of semi conductor components with time are required for vehicle project specific load cycles. The length of load cycles may range from minutes up to hours. The advantage of RC Networks and equivalent circuit models, see for example Ref. [6], is to swiftly provide the transient results by taking as input the time dependent power losses, thermal resistances and adjoining capacitances. Below demonstrates the thermal predictions stemming from a so-called Foster model outlined in Figure 11. The derivatives of the model that are used in here are referred to as H^2, Y^2 and Y^1. The suffix indicates the order by which the results are resolved in time. In the 1st order model only one link of resistor and capacitor is used. The Y models differ from the H^2 model in that the transversal thermal resistances of R_{CC} and R_{HH} are infinite and zero, respectively. These resistances are invoked at the levels of case and heat sink.

The characteristics of R and C of the models are obtained by means of optimizing the model performance against the steady state and step response results of Case 1, that are obtained with CFD. For that purpose the optimization toolbox of Matlab from Mathworks is utilized. The predictive capability of the junction temperatures in comparison to the CFD data are shown in Figure 10.

Further, the responses of the models in terms of the junction temperature, to a 60 s pulse, for the three cases of Table 1 are shown in Figure 12. For Case 1, which is representative for traction motor converters, power losses are somewhat symmetric and occur in diodes and transistors. However, in other applications where either the diodes or transistors are active, discrepancies become more noticeable. In this respect, the limitation of the Y models is that the passive junction temperature is equal to that of the active heat sink temperature. As far as the asymmetric cases are concerned, the H^2 model predicts a slightly higher active junction temperature (0.6 K), and inversely lower passive junction temperatures (-1.1 K). This is a result of the non-zero R_{HH} (7 K/kW) component and relatively high R_{CC} (55 K/kW) in the H^2 model.

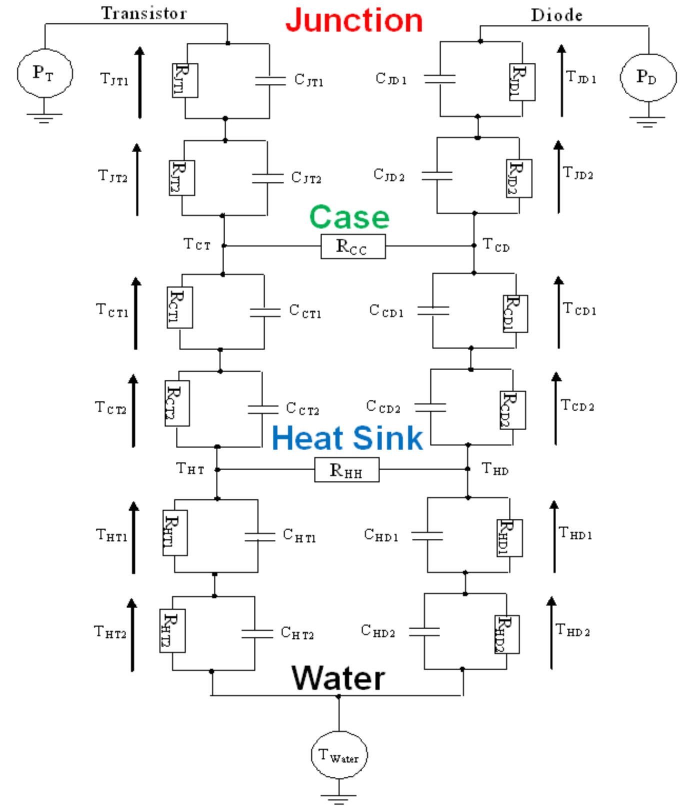

Figure 11 General Foster model of type H^2.

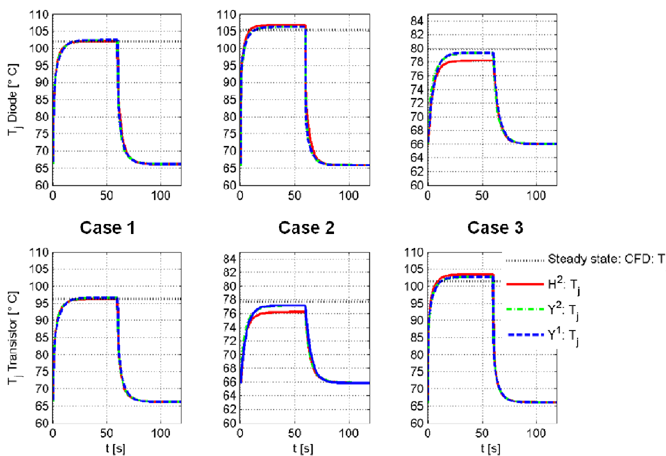

Figure 12 Response of junction temperatures for Case 1, 2 and 3 with regards to a 60 s pulse.

In the final exercise, shown in Figure 13, a real load cycle for a typical Regional vehicle is used, where liquid cooling is suitable. The agreement of results, with respect to the junction temperatures is satisfactory, in that the results for all models compare well, and in turn give similar life length predictions of the IGBT modules. Thus, for the current liquid cooled application the simplest Y^1 model suffices to describe the situation. The conclusion may change for air cooled metro applications, where the load cycle is busier and the thermal crosstalk is different.

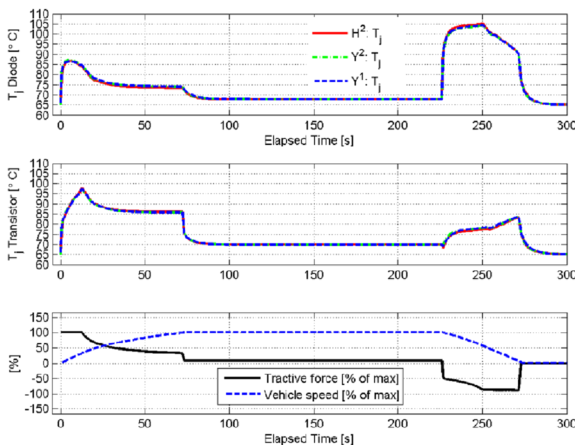

Figure 13 Response of junction temperatures with regards to a real traction motor converter application and load cycle.

SUMMARY

An experimental database for the application of liquid cooling of IGBT modules has been obtained and presented. The key results are the steady state temperatures of the base plate and heat sink for three different heat dissipating cases of the diodes and transistors.

Three dimensional CFD calculations are carried out that provide detailed results of temperature field of the IGBTs, flow inside the heat sink and conjugate heat transfer.

The results conclude that a cost efficient and accurate numerical methodology has successfully been developed. It is also described how accurate transient results of step responses for the entire system can be obtained at a reasonable computational cost. Such results are important for traction motor converters that operate with time dependent load cycles. In particular, the results from transient CFD results are suitable for generating equivalent circuit models that essentially describe the temperature field in two dimensions. Three models are examined. It is concluded that the simplest of these models is sufficient to resolve the time dependency of the junction temperatures of a typical load cycle pertinent to a regional rolling stock operation with regards to life length analysis.

ACKNOWLEDGEMENT

The authors wish to thank all colleagues at Bombardier who have contributed with experience, skills and fruitful discussions. Special thanks go to Mr. Anders Berglund for setting up and conducting the experiments.

REFERENCES

[1] Gradinger, T. and Liu, Y. 2010. Fast and Accurate Simulation of Time-Varient Air-Cooling systems. CIPS 2010, march, 16–18, 2010, Nuremberg/Germany. Paper 12.5.

[2] Ferziger, J, H. and Peri´c. Computational Methods for Fluid Dynamics. Springer. ISBN 3-540-59434-5.

[3] Menter, F.R. 1994. "Two-equation eddy-viscosity turbulence modeling for engineering applications", AIAA Journal, 32(8), pp. 1598-1605.

[4] Shih, T.-H., Liou, W.W., Shabbir, A., Yang, Z. and Zhu, J. 1994. "A New k- Eddy Viscosity Model for High Reynolds Number Turbulent Flows - Model Development and Validation", NASA TM 106721.

[5] Technical Information. IGBT-Module. FZ1500R33HE3. www.infineon.com

[6] Ottosson, J. 2013. Thermal Modelling of Power Modules in a Hybrid Vehicle Application. Doctoral Thesis in Electrical Engineering. Lund University. ISBN: 978-91-88934-61-1.